AIP | Applied Physics Letters

Shrinkage and expansion mechanisms of SiO2 elliptical membrane nanopores

Jae Won Shin, Jeong Yong Lee, Do Hyun Oh, Tae Whan Kim, and Woon Jo Cho

Citation: Appl. Phys. Lett. **93**, 221903 (2008); doi: 10.1063/1.3027062
View online: http://dx.doi.org/10.1063/1.3027062
View Table of Contents: http://apl.aip.org/resource/1/APPLAB/v93/i22
Published by the American Institute of Physics.

Shrinkage and expansion mechanisms of SiO_2 elliptical membrane nanopores

Jae Won Shin,[1] Jeong Yong Lee,[1] Do Hyun Oh,[2] Tae Whan Kim,[2,a)] and Woon Jo Cho[3]
[1]*Department of Materials Science and Engineering, KAIST, Daejeon 305-701, Republic of Korea*
[2]*Division of Electronics and Computer Engineering, Hanyang University, Seoul 133-791, Republic of Korea*
[3]*Nano Device Research Center, KIST, Seoul 136-791, Republic of Korea*

(Received 5 August 2008; accepted 25 October 2008; published online 1 December 2008)

20 nm SiO_2 elliptical membrane nanopores with various thicknesses were directly formed *in situ* by using a focused electron beam with transmission electron microscopy (TEM). The shrinkage and the expansion behaviors of the SiO_2 ellipse nanopores with different thicknesses were attributed to variations in their geometries, in particular their curvatures. The geometric mechanisms of elliptical nanopores with various thicknesses fabricated utilizing a SiO_2 membrane with a thickness gradient by using an electron beam irradiation are described on the basis of TEM images, which depend on the electron beam irradiation time. © *2008 American Institute of Physics*.
[DOI: 10.1063/1.3027062]

Nanopores have become particularly attractive due to interest in their promising applications in next-generation nanosensors because of their unique advantages of rapid electrical detection and characterization of biomolecules.[1–5] Protein-pore-based sensors fabricated utilizing organic nanopores have been utilized to discriminate various nucleic acid molecules,[6,7] to detect single-nucleotide differences,[8] and to characterize the hybridization of individual DNA strands.[9] However, the sensors based on organic nanopores have inherent problems due to poor stability of their mechanical, chemical, and electrical properties. Inorganic solid-state nanopores have been fabricated by using ionic sculpting to overcome these inherent problems of the poor stabilities of the organic nanopores.[10] Such nanopores are particularly interesting due to their promising applications, which offer the unique advantages of high stability, precise control of the diameter and the channel length, adjustable surface properties, and possible integration into devices and arrays.[11] The potential applications of nanopores based on various materials have driven extensive efforts to control precisely the sizes and the shapes of the nanopores by using various methods.[12–14] Even though studies concerning the formation of nanopores by using various methods, such as chemical modification,[15] thermal oxidation,[16] oxide deposition,[17,18] and selective area electron beam irradiation,[19] have been used to modify their shape, investigations of the shrinkage and the expansion mechanisms of SiO_2 elliptical membrane nanopores have not been performed yet. Size control and shape modification of solid-state nanopores are necessary to fabricate high-efficiency nanodevices.

This letter reports the shrinkage and the expansion mechanisms of SiO_2 elliptical membrane nanopores with various thicknesses. The shrinkage and expansion behaviors of the geometries of elliptical nanopores with various thicknesses fabricated utilizing a SiO_2 membrane with a thickness gradient by using electron beam irradiation are described on the basis of transmission electron microscopy (TEM) images.

An amorphous SiO_2 layer with a 200 nm thickness was deposited on a *p*-Si substrate by using a rf magnetron sputtering method. Polycrystalline SiO_2 was used as a target material. The substrate temperature, the working pressure, the Ar and O_2 flow rate, the rf power, and the O_2 concentration in the Ar atmosphere for the formation of the SiO_2 layers were 300 °C, 5 mTorr, 10 SCCM (SCCM denotes cubic centimeter per minute at STP), 100 W, and 30%, respectively. The samples for the TEM measurements were prepared by cutting and polishing with diamond paper to a thickness of approximately 30 μm. The SiO_2 membrane with a thickness gradient under 10° was prepared by ion milling with a source gun, as shown in Fig. 1(a). TEM specimens were loaded into a Tecnai F30 S-twin TEM, and approximately 20 nm elliptical nanopores with various thicknesses were directly formed by using a focused electron beam with a size of 20 nm in the

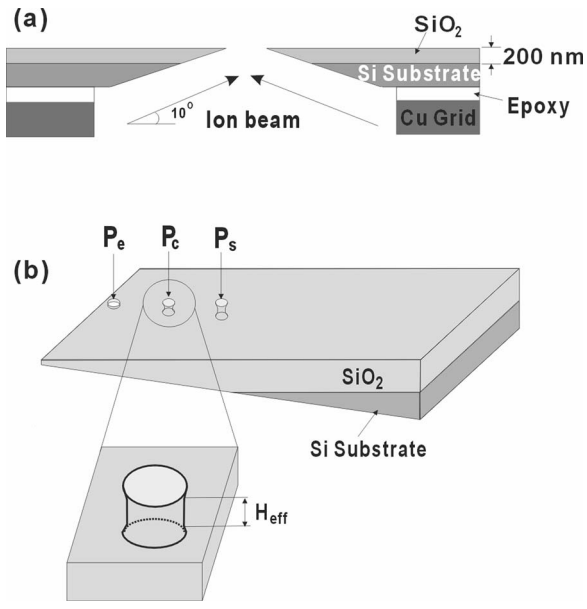

FIG. 1. Schematic diagrams for the (a) SiO_2 membrane with a thickness gradient prepared by argon-ion milling with an ion source gun located at the lower side and (b) nanopores with various thicknesses directly drilled by using a focused electron beam with *in situ* TEM. P_e, P_c, and P_s represent the expansion of the nanopore, the stable nanopore with a critical thickness, and the shrinkage of the nanopore, respectively.

a)Author to whom correspondence should be addressed. Electronic mail: twk@hanyang.ac.kr.

TEM equipment. Then, an electron beam with low-intensity electrons irradiated the outer regions (approximately 1 μm^2) of the elliptical nanopores to induce a viscous flow of SiO_2.

The irradiation of focused high-intensity electrons (above 10^8 e/nm^2) breaks the bonding of Si and O atoms and causes atoms to be sputtered away into the vacuum, resulting in the drilling of the nanopore in SiO_2 membrane. However, when low-intensity electrons irradiate the large area of approximately 1 μm^2, another mechanism dominates. The low-intensity electron beam ($10^4 \sim 10^6$ e/nm^2) irradiated on the large area generates a viscous flow in the amorphous SiO_2 layer resulting from the operation of knock-on displacement due to momentum transfer to the SiO_2 molecules rather than the sputtering effect.[16,20,21] The magnitude of the expansion and the shrinkage of the nanopores are determined by using the induced mass flow rates due to the minimization of the surface free energy of the SiO_2 layer. When the thickness of the nanopore is smaller than its critical thickness, the surface free energy decreases with the increasing diameter, resulting in an expansion of the nanopore. However, when the thickness of the nanopore is larger than its critical thickness, the surface free energy decreases with the decreasing diameter, resulting in a shrinkage of the nanopore. A stable nanopore with a critical thickness maintains a constant diameter during electron beam irradiation. Because the circular nanopores fabricated in the specimen have various thicknesses, the region with a critical thickness can be identified by observing circular nanopore behaviors with a diameter of approximately 22 nm (± 1 nm) during electron beam irradiation, as shown in Fig. 1(b). The effective height of the stable circular nanopore with a critical thickness, that of the shrinking circular nanopore, and that of the expanding circular nanopore are approximately 16.6, 20.5, and 8.51 nm, respectively, as determined from the tilting method. A focusing electron beam with an elliptical shape was formed by aligning the condenser stigmatism. The elliptical nanopores with a critical size of major axis of 25.5 nm (± 1 nm) and a minor axis of 20.5 nm (± 1 nm) in SiO_2 membrane with thinner, critical, and thicker thicknesses were fabricated by using a focusing electron beam with an elliptical shape nearby circular nanopores with thinner, thicker, and critical thicknesses. The ratio of the major axis to the minor axis (a/b) is 1.15. Because the elliptical nanopores were fabricated nearby circular nanopores, the elliptical nanopores with thinner, critical, and thicker thicknesses have almost the same thickness as circular nanopores with thinner, thicker, and critical thicknesses.

The size and the shape for elliptical nanopores with thinner, thicker, and critical thicknesses for various electron beam irradiation times are shown in Figs. 2(a)–2(d), Figs. 2(e)–2(h), and Figs. 2(i)–2(l), respectively. The a/b ratios of elliptical nanopores with different thicknesses as functions of the electron beam irradiation time are shown in Fig. 2(m). While the a/b ratio of an elliptical nanopore with a thinner thickness decreases to one with the increasing electron beam irradiation time, resulting in the formation of nanopores with a perfectly circular cross section, the a/b ratios of elliptical nanopores with critical and thicker thicknesses increase, resulting in the formation of more compressive elliptical nanopores.

The mass flow rate related to the surface curvature should be considered to describe clearly the behavior of elliptical nanopores. The expansion and the shrinkage behaviors of the elliptical nanopores are determined by using the induced mass flow rates due to the minimization of the surface free energy of the SiO_2 layer. Since the area of the ellipse nanopore is much smaller than that of the electron irradiated area of approximately 1 μm^2, the local stress field perpendicular to the virtual perfect cylinder might radiate in all directions during the expansion of the nanopore, as shown in Fig. 3(a). The virtual perfect circle is straightened to simplify the expansion stress field, resulting in the existence of the stress along the same direction, as shown in Figs. 3(b) and 3(c). When the nanopores expand, the stress existing on the major axis localizes due to the positive surface curvature along the direction of the stress field, resulting in a larger mass flow rate outside the nanopores along the major axis. However, the stress along the minor axis is dispersed due to the negative surface curvature along the direction of the stress field, resulting in a smaller mass flow rate outside the nanopores along the minor axis. The a/b ratio of the elliptical nanopore increases during the expansion of the nanopores due to the formation of a more compressive elliptical nanopore due to the surface curvature.

When the nanopore shrinks, the local stress field perpendicular to the perfect cylinder is focused on the axis of the nanopore from all directions, as shown in Fig. 3(d). The stress along the major axis is dispersed during the shrinkage of the elliptical nanopore due to the negative surface curvature along the direction of the stress field, as shown in Fig.

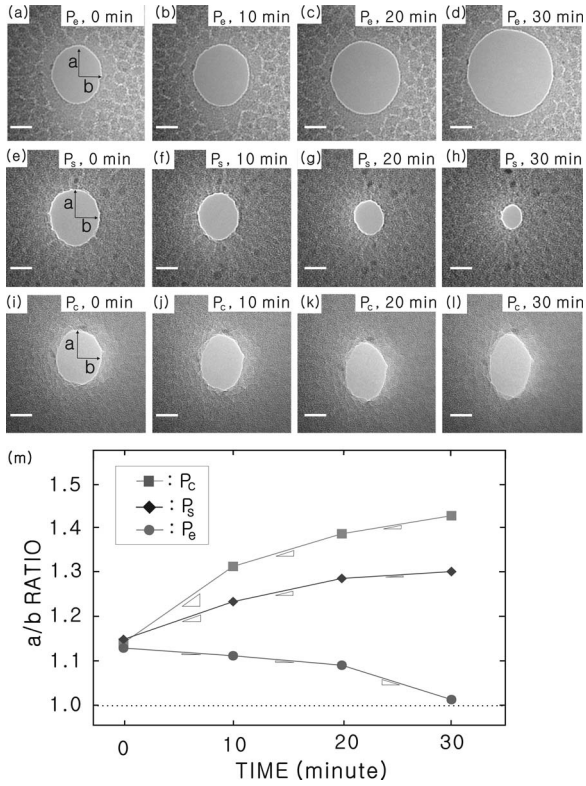

FIG. 2. TEM images of thinner elliptical nanopores electron irradiated for (a) 0, (b) 10, (c) 20, or (d) 30 min, of elliptical nanopores with a critical thickness electron irradiated for (e) 0, (f) 10, (g) 20, or (h) 30 min, of thicker elliptical nanopore electron irradiated for (i) 0, (j) 10, (k) 20, or (l) 30 min, and (m) a/b ratios as functions of the irradiation time for elliptical nanopores. The scale bar corresponds to 10 nm. P_e, P_c, and P_s represent the expansion of the nanopore, the stable nanopore with a critical thickness, and the shrinkage of the nanopore, respectively.

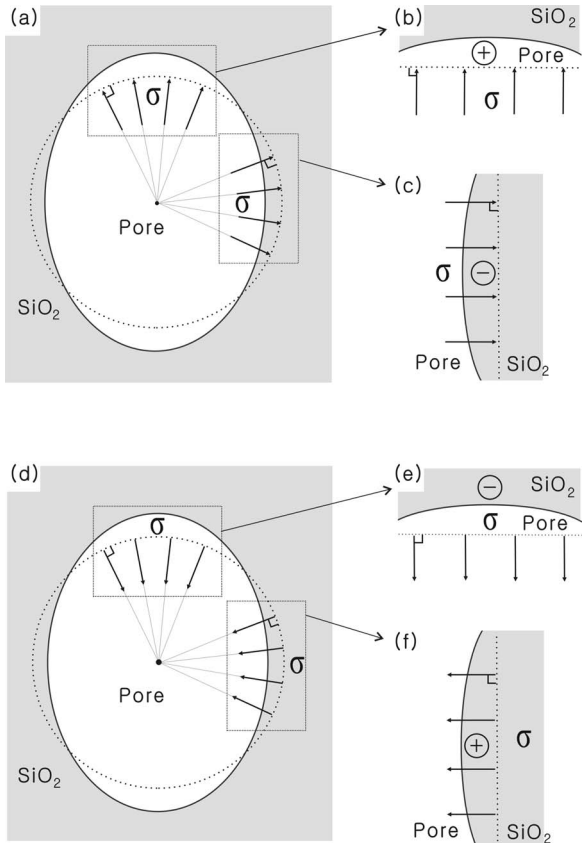

FIG. 3. Schematic diagrams for the stress fields in [(a)–(c)] expanding elliptical nanopores and [(d)–(f)] shrinking nanopores.

3(e), resulting in a smaller mass flow rate to the axis of the nanopore along the major axis. However, the stress along the minor axis is localized due to the positive surface curvature along the direction of the stress field, as shown in Fig. 3(f), resulting in a larger mass flow rate along the minor axis of the nanopore. The a/b ratio of the elliptical nanopore increases during the shrinkage of the nanopore. Therefore, the a/b ratio of the elliptical nanopore increases during the expansion and shrinkage processes of the nanopore due to the magnitude of the mass flow rate and the surface curvature, with the formation of a preferentially compressive elliptical nanopore, a factor of 1. However, because a perfect cylinder has the lowest surface area per unit volume, the surface energy decreases due to the formation of a perfect cylinder whose a/b ratio is 1, a factor of 2.

These two factors should be considered to describe exactly the behaviors of elliptical nanopores. When the nanopore expands, because the surface area of the nanopore increases, the surface energy is minimized in comparison with the magnitude of the mass flow rate due to the surface curvature dominantly affecting the expansion process of an elliptical nanopore, resulting in a decrease in the a/b ratio of the elliptical nanopore during the expansion process, as shown in Figs. 1(a)–1(d) and 1(m). However, because the surface area of the nanopore decreases during the shrinkage of the nanopore, the effects of the magnitude of the mass flow rate due to the surface curvature dominate the increase in the a/b ratio of the elliptical nanopore during the nanopore shrinkage process, resulting in the formation of the more compressive elliptical nanopore, as shown in Figs. 1(e)–1(h) and 1(m). When the size of the elliptical nanopore with a critical thickness is approximately 20 nm, the effect of the mass flow rate due to the surface curvature dominates the behavior of the elliptical nanopore, resulting in an increase in the a/b ratio during the electron beam radiation, as shown in Figs. 1(i)–1(m).

In summary, 20 nm SiO_2 ellipse nanopores with various thicknesses were directly formed *in situ* by using a focused electron beam with TEM equipment. The TEM image showed that the a/b ratio of the elliptical nanopore with a thinner thickness decreased to 1, with an increase in the rate of decrease in the a/b ratio resulting from the formation of a perfect circle. The a/b ratio of the elliptical nanopores with a critical or thicker thickness increased with a decrease in the rate of increase resulting from the formation of a preferentially compressive elliptical nanopore. The shrinkage and the expansion behaviors of the elliptical nanopore with the increasing electron beam irradiation time were attributed to the variations in their geometry.

This work was supported by the Korea Science and Engineering Foundation (KOSEF) grant funded by the Korean Government (MEST) (Grant No. R0A-2007-000-20044-0), and this work was also supported by a grant (Code #: 08K1501-01210) from the Center for Nanostructured Materials Technology under 21st Century Frontier R&D Programs of the Minsitry of Education, Science and Technology, Korea.

[1] J. J. Kasianowicz, E. Brandin, D. Branton, and D. W. Deamer, Proc. Natl. Acad. Sci. U.S.A. **93**, 13770 (1996).
[2] J. Li, M. Gershow, D. Stein, E. Brandin, and J. A. Golovchenko, Nature Mater. **2**, 611 (2003).
[3] H. Chang, F. Kosari, G. Andreadakis, M. A. Alam, G. Vasmatzis, and R. Bashir, Nano Lett. **4**, 1551 (2004).
[4] A. J. Storm, C. Storm, J. H. Chen, H. Zandbergen, J. F. Joanny, and C. Dekker, Nano Lett. **5**, 1193 (2005).
[5] R. M. M. Smeets, U. F. Keyser, D. Krapf, M.-Y. Wu, N. H. Dekker, and C. Dekker, Nano Lett. **6**, 89 (2006).
[6] M. Akeson, D. Branton, J. J. Kasianowicz, E. Brandin, and D. W. Deamer, Biophys. J. **77**, 3227 (1999).
[7] A. Meller, L. Nivon, E. Brandin, J. Golovchenko, and D. Branton, Proc. Natl. Acad. Sci. U.S.A. **97**, 1079 (2000).
[8] W. Vercoutere, S. Winters-Hilt, H. Olsen, D. Deamer, D. Haussler, and M. Akeson, Nat. Biotechnol. **19**, 248 (2001).
[9] S. Howorka, L. Movileanu, O. Braha, and H. Bayley, Proc. Natl. Acad. Sci. U.S.A. **98**, 12996 (2001).
[10] J. Li, D. Stein, C. McMullan, D. Branton, M. J. Aziz, and J. A. Golovchenko, Nature (London) **412**, 166 (2001).
[11] C. Dekker, Nat. Nanotechnol. **2**, 209 (2007).
[12] A. Mara, Z. Siwy, C. Trautmann, J. Wan, and F. Kamme, Nano Lett. **4**, 497 (2004).
[13] D. Fologea, J. Uplinger, B. Thomas, D. S. McNabb, and J. Li, Nano Lett. **5**, 1734 (2005).
[14] A. J. Storm, J. H. Chen, X. S. Ling, H. W. Zandbergen, and C. Dekker, Nature Mater. **2**, 537 (2003).
[15] G. Wang, B. Zhang, J. R. Wayment, J. M. Harris, and H. S. White, J. Am. Chem. Soc. **128**, 7679 (2006).
[16] A. J. Storm, J. H. Chen, X. S. Ling, H. W. Zandbergen, and C. Dekker, J. Appl. Phys. **98**, 014307 (2005).
[17] J. Nilsson, J. R. I. Lee, T. V. Ratto, and S. E. Letant, Adv. Mater. (Weinheim, Ger.) **18**, 427 (2006).
[18] C. Danelon, C. Santschi, J. Brugger, and H. Vogel, Langmuir **22**, 10715 (2006).
[19] W. M. Zhang, Y. G. Wand, J. Li, J. M. Xue, H. Ji, Q. Ouyang, J. Xu, and Y. Zhang, Appl. Phys. Lett. **90**, 163102 (2007).
[20] P. M. Ajayan and S. Tijima, Philos. Mag. Lett. **65**, 43 (1992).
[21] M. J. Kim, M. Wanunu, D. D. Bell, and A. Meller, Adv. Mater. (Weinheim, Ger.) **18**, 3149 (2006).